International Journal of Fatigue 198 (2025) 108937

Contents lists available at ScienceDirect

International Journal of Fatigue

journal homepage: www.elsevier.com/locate/ijfatigue

Assessment of fatigue crack initiation after overloads with substructure-sensitive crystal plasticity

Shahram Dindarlou [a], Gustavo M. Castelluccio [b,*]

[a] University of Twente, Netherlands
[b] School of Aerospace, Transport and Manufacturing, Cranfield University, Cranfield, UK

ARTICLE INFO

Keywords:
Crystal plasticity
Mesoscale structure
Overload effects
Cyclic deformation history

ABSTRACT

Microstructure-sensitive fatigue initiation prognosis approaches typically assume uniform periodic loading and often overlook in-service overloads, which increase uncertainty and reduce life prediction accuracy. Similarly, certification efforts rarely evaluate experimentally the impact of different overloads due to the prohibitive costs. Therefore, predictive models that estimate overload effects on fatigue initiation damage without extensive experimental data are valuable to improve prognosis approaches. However, the literature lacks microstructure-sensitive approaches capable of assessing overload effects with models that simultaneously predict monotonic and cyclic responses without recalibration.

This work presents a novel strategy to predict the effects of overloads on early cyclic damage by evaluating the refinement dislocation structures. A substructure-based crystal plasticity approach relies on independent parameterizations from monotonic and cyclic loading to predict overload responses, without requiring additional experiments. The model agreement with macroscale experiments was further validated by comparing dominant mesoscale structures after overloads in single- and poly-crystals for metals and alloys. The analysis also identified overload-resistant crystal orientations and demonstrated that overloads increase the likelihood of initiating fatigue cracks in low apparent Schmid factor grains under low-amplitude fatigue. We conclude by discussing the value of material-invariant mesoscale parameters to rank overloads effect for materials and loading conditions for which no experiments are available.

1. Introduction

Fatigue damage is a prevalent cause of failure of industrial components [1], and it is driven by repetitive mechanical loads. Most commonly, experimental, theoretical, or numerical fatigue damage assessments assume a uniform periodic load, overlooking the variable mechanical excursions that occur during service. However, experiments have demonstrated that non-periodic cyclic deformation can have significant effects on fatigue life [2–6]. Hence, cyclic deformation analyses that exclude excursions outside continuous periodic loads are prone to mispredicting realistic industrial service conditions. Notably, overloads can either accelerate or slow down fatigue damage [7–10], making their understanding valuable for improving safety and achieving economic benefits from life extensions. In particular, the understanding of overloads effects on fatigue crack initiation is notably understudied given the experimental difficulties [11].

Much of the research related to non-uniform cyclic loading has focused on quantifying crack growth rate retardation or acceleration [8,9,12–14], which have been explained by residual stresses, crack closure, or damage ahead of the crack. Evidently, a prerequisite to modeling crack initiation is a constitutive model capable of predicting the crystallographic behavior upon a change in loading conditions. Although a few attempts have addressed these needs [7,8,12,13], no systematic understanding has been developed for modeling the role of cyclic deformation followed by an overload/overstrain at the grain level. Some valuable efforts [15,16] have relied on calibrating multiple parameters or have made simple predictions [17,18] with fatigue models not validated for single crystals or overloads. However, the literature lacks a general microstructure-sensitive approach that can predict seamlessly (e.g., without recalibration) monotonic and cyclic responses over a wide range of plastic strain amplitudes and multiple materials. This deficit is even more noticeable for modeling single-crystal mechanical responses, which are a means to validate models for polycrystals texture analysis. Hence, there is a need to advance mechanistic crystal plasticity approaches that estimate the response of materials beyond a few specific loading sequences used for calibration. These models can estimate damage potential under service conditions that have not

* Corresponding author.
E-mail address: castellg@cranfield.ac.uk (G.M. Castelluccio).

https://doi.org/10.1016/j.ijfatigue.2025.108937
Received 27 January 2025; Received in revised form 12 March 2025; Accepted 12 March 2025
Available online 3 April 2025
0142-1123/Crown Copyright © 2025 Published by Elsevier Ltd. This is an open access article under the CC BY license (http://creativecommons.org/licenses/by/4.0/).

been directly tested. Moreover, they can support the design of material attributes such as texture and grain morphology to mitigate or take advantage of overload effects on cracking.

The cyclic response of metallic materials strongly depends on their microstructure and history, which may lead to cyclic softening or hardening [19]. After a few hundred or thousands of cycles (depending on the applied strain) dislocation hardening tend to saturate and the stress–strain loop stabilize. In single face FCC materials, this response has been related [20] to the formation of stable dislocation structures, which control forest dislocation hardening. However, experiments [3,4,21,22] have demonstrated that a significant overload can destabilize and refine dislocation structures. These structural changes, controlled by the mesoscale, affect the behavior ahead of a crack and the macroscopic cyclic response. For example, Marnier and coworkers [3] demonstrated that the transformation from elongated to equiaxed dislocation structures after an overload is the mechanism responsible for the increase in the subsequent cyclic stress. Hence, the modeling of mesoscale structural changes can support predictive approaches that can be validated at the macroscopic and mesoscopic length scales.

Castelluccio and McDowell [23] formulated a substructure-sensitive crystal plasticity (CP) model to compute the macroscopic cyclic response of FCC single- and poly-crystals. Their work incorporates mesoscale parameters with known uncertainty that interrelate external stresses, internal stresses, and dislocation structure morphologies. However, their model assumes stable saturated structures formed by cyclic loading and cannot capture the structural changes of monotonic overloads. Their work was further extended by Ashraf and Castelluccio [20] to model cyclic history effect across temperatures by parameterizing the evolution of dislocation structures. Dindarlou and Castelluccio [24] further developed substructure-sensitive approaches for monotonic loading with a CP model based on the evolution of mesoscale structures evolution. This model successfully predicted both micro- and macro-scale behaviors of single and polycrystalline for numerous FCC materials with a single set of material-invariant parameters. Moreover, they demonstrated [25] the ability to predict the response of engineering alloys single crystal data without the need for mesoscale recalibration. Notably, both monotonic [24] and cyclic [20] models only differ on the parameterization of the shape and dimensions of dislocation structures, which are material independent but loading dependent; atomic unit processes parameters such as dislocation glide energy is identical in both models (and strongly material dependent). Hence, these results suggest that a general approach for overloads can be produced without the need for additional parameterization by assessing the stability of cyclic dislocation structures after a mechanical monotonic overload.

This work integrates monotonic and cyclic CP models without any reparameterization to predict the meso- and macro-scale response of FCC materials subjected to cyclic loading including overloads, including single- and poly-crystals. We demonstrate that previously optimized parameters for monotonic and cyclic responses can predict overload responses without the need for recalibration. The same set of mesoscale parameters were employed to blindly predict the response of NiCr alloys under cyclic loading with overload. Furthermore, the predicted macroscopic responses were explained by mesoscale structure changes during overload in agreement with the experiments ranging from macro- and meso-scales. Finally, we employ the approach to study the influence of overloads on fatigue crack initiation in polycrystals by means of Fatigue Indicator Parameters (FIPs).

2. Crystal plasticity finite element model

We briefly present the crystal plasticity formulation, which is similar to those proposed earlier for monotonic [25] and cyclic loading [20]. We consider the large deformation multiplicative decomposition of the strain gradient $\mathbf{F}$ [26,27], which is composed by elastic, $\mathbf{F^e}$, and plastic, $\mathbf{F^p}$, components, i.e.,

$$\mathbf{F} = \mathbf{F^e}.\mathbf{F^p}. \tag{1}$$

The time derivative of plastic deformation gradient, $\dot{\mathbf{F}}^{\mathbf{p}}$, relates to the isoclinic intermediate configuration plastic velocity gradient, $\mathbf{L^p}$, such that

$$\dot{\mathbf{F}}^p = \mathbf{L^p}.\mathbf{F^p} = \sum_{\alpha=1}^{N_{sys}} \dot{\gamma}^\alpha(\mathbf{s}^\alpha \otimes \mathbf{m}^\alpha), \tag{2}$$

where $\otimes$ is dyadic product, $\dot{\gamma}$ is shear rate while $\mathbf{s}^\alpha$ and $\mathbf{m}^\alpha$ correspond to the slip direction and slip plane normal of slip system α, respectively. Elastic deformation gradient is calculated,

$$\mathbf{F^e} = \mathbf{F}.(\mathbf{F^p})^{-1}, \tag{3}$$

to compute elastic Green strain tensor,

$$\mathbf{E^e} = \frac{1}{2}\left[(\mathbf{F^e})^T.\mathbf{F^e} - \mathbf{I}\right], \tag{4}$$

this tensor is then multiplied by fourth rank elasticity tensor with cubic symmetry, $\mathbf{C}$, to compute the 2nd Piola–Kirchhoff stress,

$$\boldsymbol{\sigma}^{\mathbf{PK2}} = \mathbf{C} : \mathbf{E^e}, \tag{5}$$

while the Cauchy stress is computed as,

$$\boldsymbol{\sigma} = \frac{1}{det(\mathbf{F^e})}\left[\mathbf{F^e}.\boldsymbol{\sigma}^{\mathbf{PK2}}.(\mathbf{F^e})^{-1}\right]. \tag{6}$$

Following Orowan [28], the shear rate, $\dot{\gamma}^\alpha$, in Eq. (2) relates to the mobile dislocation densities, ρ_m^α,

$$\dot{\gamma}^\alpha = \rho_m^\alpha b v, \tag{7}$$

in which b and v are magnitudes of Burgers vector and mean mobile dislocations velocity.

Assuming that dislocation glide is a thermally activated process controlled by transition state theory [29], we compute the probability of a dislocation to overcome an obstacle as,

$$v = l\nu exp\left(\frac{-\Delta G}{k_B T}\right), \tag{8}$$

where l, ν, k_B and T are the average distance between dislocations barriers, the attempt frequency, the Boltzmann constant, and the temperature, respectively. Furthermore, ΔG corresponds to the Gibbs free activation energy of a dislocation, which has been parameterized though multiple approaches [30–33]. Here, we follow the formulation proposed by Kocks et al. [34], i.e.,

$$\Delta G = F_0\left(1 - \left[\frac{\tau_{eff}}{s_0}\right]^p\right)^q, \tag{9}$$

in which F_0 is the glide activation energy at 0 K, s_0 is thermal stress and p and q are profile parameters. Combining Eqs. (7), (8) and (9) we obtain the flow rule,

$$\dot{\gamma}^\alpha = \rho_m^\alpha b l_{struct} v \exp\left(-\frac{F_0}{k_B T}\left\langle 1 - \left[\frac{\left\langle\left|\tau_{eff}^\alpha\right|\right\rangle}{s_t^0 \frac{\mu}{\mu_0}}\right]^p\right\rangle^q\right) \mathrm{sgn}\left(\tau^\alpha - B^\alpha\right), \tag{10}$$

where μ and μ_0 are the shear modulus at temperature T and $0K$ and the Macaulay brackets follows $\langle G\rangle = 0$ if $G \le 0$ or $\langle G\rangle = G$ if $G > 0$. We assume that the substructures characteristic length (l_{struct}) is the limiting factor for the mobile dislocation mean free paths and varies for different orientations and loading history [35].

Eq. (10) relates the local plastic shear rate induced by the local effective stress, τ_{eff}^α, driving dislocation glide. This stress relate the mesoscale (finite element) level shear stress, τ^α with the atomic unit process driving force such that,

$$\tau_{eff}^\alpha = \left\langle|\tau^\alpha - B^\alpha| - S^\alpha\right\rangle, \tag{11}$$

in which S^α corresponds to the local athermal stress and B^α to the intragranular back stress, which is controlled by the dimension and morphology of dislocation structures.

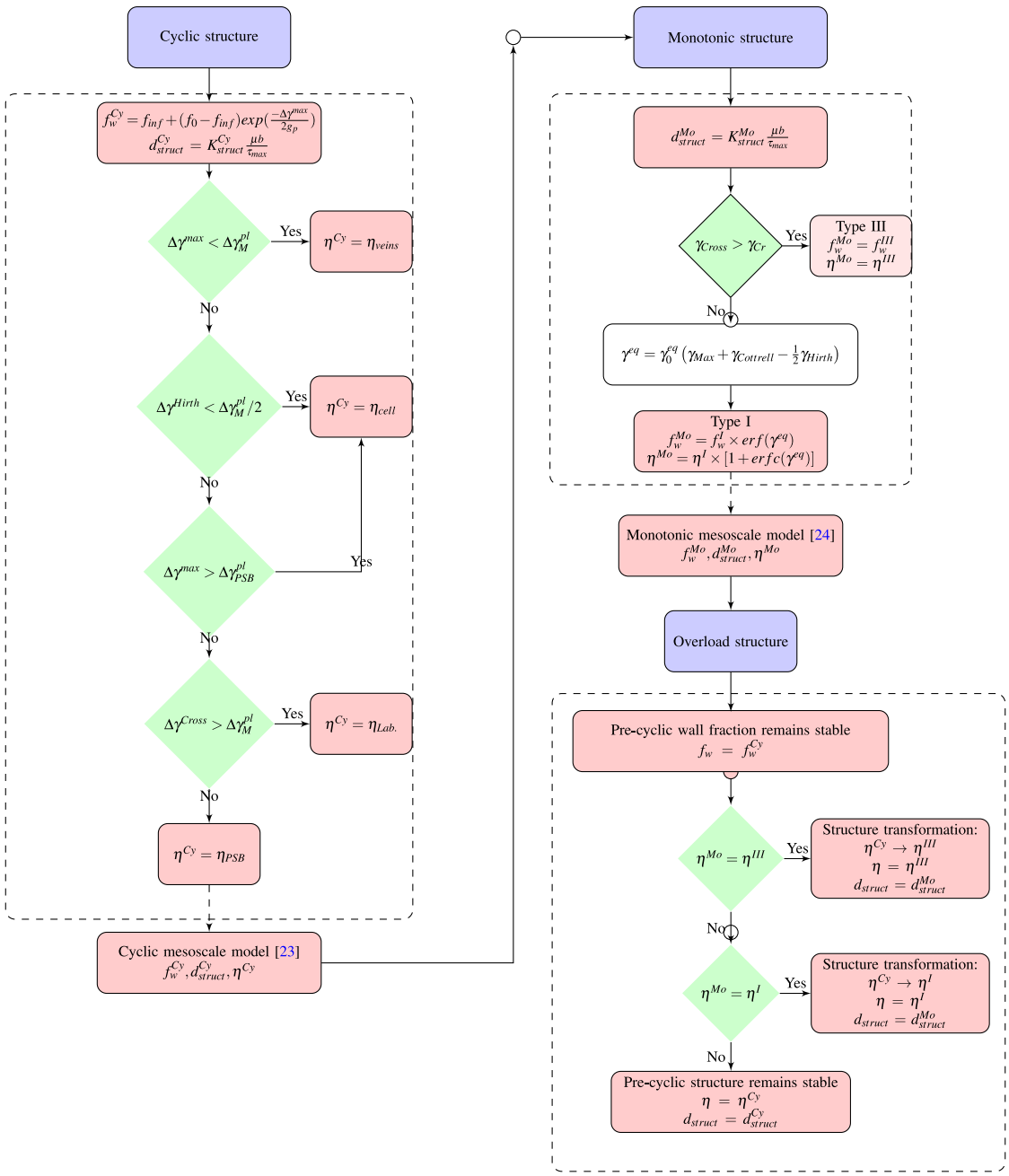

Fig. 1. The cyclic (top left), the monotonic (top right) and the overload (bottom right) models to predict mesoscale structures. The overload model equates that in the post-overload cycles, the pre-cyclic wall fraction remains stable ($f_w = f_w^{Cy}$). If the pre-cyclic structure transforms to $TypeIII$ or $TypeI$ in monotonic model, then it will remain stable in post overload cycles, otherwise, the pre-cyclic structure remain unchanged (no overload effect).

2.1. Substructure-based back stress

Inelastic deformation of single phase FCC metallic materials results in production of dislocations that localize into immobile structures (walls) that constrain the mobile dislocations in channels in between. Since the dislocation density within the walls is normally much higher than in the channels, the plastic deformation within walls is negligible. Thus, elastically deformed walls and plastically deformation channels produce a residual intragranular back stress. Castelluccio and McDowell [23] propose a mean field back stress rate based on the constraint induced by walls on dislocation glide,

$$\dot{B}^{\alpha} = \frac{f_w}{1 - f_w} \frac{2\mu(1 - 2S_{1212})}{1 + 4S_{1212} f_{Hill}^{S}} \dot{\gamma}^{\alpha}, \tag{12}$$

where the Hill factor under shear deformation, f_{Hill}^{S}, has been defined as the instantaneous macroscopic plastic deformation tangent, i.e

$$f_{Hill}^{S} = \frac{1}{2} \frac{d\gamma_p}{d\sigma} \tag{13}$$

And the f_w is the dislocation wall volume fraction and,

$$S_{1212} = \frac{\pi\eta^2 + (\eta^2 - 1.75 - 2\nu_p\eta^2 + 2\nu_p)C_{12}}{8\pi(1 - \nu_p)(\eta^2 - 1)} \tag{14}$$

is the Eshelby tensor component for a prolate spheroid [36] with

$$C_{12} = \frac{2\pi\eta(\eta\sqrt{\eta^2 - 1} - cosh^{-1}(\eta))}{\sqrt{(\eta^2 - 1)^3}} \tag{15}$$

and

$$\nu_p = \frac{\nu + \frac{2}{3}\mu(1+\nu)f^S_{Hill}}{1 + \frac{4}{3}\mu(1+\nu)f^S_{Hill}}. \tag{16}$$

The wall and channel model is applicable to monotonic and cyclic loadings, which makes Eq. (12) sound for both loadings conditions. However, different loading conditions result in various dislocation structures [23,24], which need to be parameterized for monotonic and cyclic loadings. Under cyclic conditions, Castelluccio and McDowell [23] parameterized the evolution of the saturated cyclic wall fraction (f_w^{Cy}) as,

$$f_w^{Cy} = f_{inf} + (f_0 - f_{inf})exp(\frac{-\Delta\gamma^{max}}{2g_p}), \tag{17}$$

where $\Delta\gamma^{max}$ is the maximum crystallographic shear strain, $g_p = 0.002$ is a normalization parameter and f_0 and f_{inf} are initial and saturated walls fractions, respectively, which can be measured in experiments [37].

Under monotonic loading, Dindarlou and Castelluccio [24] assumed $S_{1212} = 0.24$ for all cases and assimilated the evolution of wall fraction akin to a phase transformation computed by,

$$f_w^{Mo} = f_w^i \times erf(\gamma^{eq}), \tag{18}$$

where f_w^i is the wall fraction for Type I, II and III structure [24]. Furthermore, γ^{eq} is the equivalent shear and computed as,

$$\gamma^{eq} = \gamma_0^{eq}\left(\gamma_{Max} + \gamma_{Cottrell} - \frac{1}{2}\gamma_{Hirth}\right), \tag{19}$$

in which $\gamma_{Cottrell}$, γ_{Hirth} and γ_{Max} are accumulated shears in Cottrell, Hirth and primary slip systems, respectively ($\gamma_0^{eq} \approx 10$). Further details can be found in refs [20,24,25]

2.2. Substructure-based athermal stress

For both monotonic and cyclic, the athermal stress is computed as the sum of the stress required to bow-out dislocations from a sessile wall and the colinear dislocation–dislocation interaction strength [23],

$$S^\alpha = \alpha_{LE}\frac{\mu b}{2d_{struct}} + \mu b\sqrt{\alpha_{ii}\rho^\alpha}, \tag{20}$$

in which α_{LE} is the dislocation line energy coefficient, d_{struct} is the wall spacing, and $\alpha_{ii} \approx 0.1$ is the colinear dislocation interaction parameter. Eq. (20) represents hardening in the channel due to colinear dislocations. Interactions among different slip systems (latent hardening) results in locks that refine the dislocation structure, and are implicitly considered by taking into account the evolution of the dislocation structure (e.g., f_w and d_{struct} in Eq. (20)).

The mobile dislocations density (ρ^α) evolves with the balance between dislocation multiplication, annihilation and cross slip such that [23],

$$\dot{\rho}^\alpha = \frac{K_{multi}}{bl_{struct}}|\dot{\gamma}^\alpha| - \frac{2y_s^{edge}}{b}\rho^\alpha|\dot{\gamma}^\alpha| + \nu_G\frac{d_{struct}}{d_0}\left(\phi_{cs}\sum_{\beta=1(\beta\neq\alpha)}^{N}\rho^\beta e^{\left(-V_{cs}^\alpha\frac{\frac{\mu b}{4\pi y_s^{screw}}-|\tau^\alpha - B^\alpha|}{K_BT}\right)} - (1-\phi_{cs})\sum_{\beta=1(\beta\neq\alpha)}^{N}\rho^\alpha e^{\left(-V_{cs}^\beta\frac{\frac{\mu b}{4\pi y_s^{screw}}-|\tau^\beta - B^\beta|}{K_BT}\right)}\right). \tag{21}$$

Here, $K_{multi} \approx 1$ is a geometric factor that scales the number of dislocations produced after applying a certain plastic shear strain while y_s^{edge} and y_s^{screw} are the annihilation distances for edge and screw dislocations, respectively. Cross-slip efficiency parameter $\phi \approx 0.5$ quantifies the likelihood for dislocation annihilation while cross-slipping and V_{cs} represents cross slip activation volume. We note that to accelerate cyclic saturation, the dislocation density evolution production term in Eq. (21) was increased by a factor of ten, during the first ten loading cycles (200 experimental cycles = 10 × 20 simulation cycles).

The mean spacing of sessile dislocations walls, d_{struct}, is calculated assuming the so-called similitude relation for both cyclic and monotonic conditions [38,39],

$$d_{struct} = K_{struct}\frac{\mu b}{\tau_{max}}, \tag{22}$$

in which τ_{max} is the maximum shear stress among all slip systems, K_{struct} is similitude coefficient. Sauzay et al. [38] analyzed myriads TEM images of structures under monotonic and cyclic loadings and reported that the value of K_{struct} for monotonic loading is almost twice of the cyclic ($K_{struct}^{Mo} \approx 2.0 \times K_{struct}^{Cy}$). In all cases, these constants are seemingly identical for a numerous FCC materials (i.e., material invariant).

Castelluccio and McDowell [23] further proposed that the dislocation mean free path l_{struct} is limited by the structure such that,

$$l_{struct} = \eta d_{struct}, \tag{23}$$

where the substructure aspect ratio, η, is a mesoscale parameter that describes dislocation structure morphologies and depends on the crystallographic orientation and deformation level [40]. Stable structures under monotonic and cyclic loading conditions have different characteristic parameterization of η. For example, Castelluccio and McDowell [23] formulated η for cyclic loading, based on accumulated plastic shear among slip systems. They proposed that if maximum plastic shear amplitude among all slip systems was lower than a critical value ($\Delta\gamma^{max} < \Delta\gamma_M^{pl}$ [41]), then the dominated saturated structure corresponds to veins with $\eta \approx 50$. If the most active slip system surpasses $\Delta\gamma_M^{pl}$ while the plastic shear amplitude on planes associate to Hirth locks is lower than a predefined value ($\Delta\gamma^{Hirth} < \Delta\gamma_M^{pl}/2$), or maximum if the maximum shear amplitude is larger than the required shear for PSB formation ($\Delta\gamma^{max} > \Delta\gamma_{PSB}^{pl}$), then the structure becomes cells with $\eta = 1.0$. For the crystals with none of the above conditions, the labyrinthic structure with $\eta = 5$ is dominant for profuse cross slip case ($\Delta\gamma^{Cross} > \Delta\gamma_M^{pl}$) and PSB structures with $\eta \approx 15$ for low cross slip conditions. A flow chart explaining the identification of the cyclic structures is shown in the top left of Fig. 1.

For monotonic loading condition, Dindarlou and Castelluccio [24] proposed an error function form analogous to a phase transformation, i.e.,

$$\eta^{Mo} = \eta^I \times \left[1 + erfc(\gamma^{eq})\right], \tag{24}$$

where η^I is the aspect ratio of elongated cell structure and γ^{eq} is explained in Eq. (19). A summary of this strategy to identify the structure under monotonic models is shown in the top right of Fig. 1. Finally, we note that the model accounts for size effects by restricting l_{struct} to be smaller than the grain size, effectively capturing the behavior of crystals and grains larger than 100 μm.

2.3. Dislocation substructures stability under combine cyclic and monotonic overload

The production and annihilation of dislocations during deformation result in evolving structures with different metastablility. For example, Dhers [42] studied the cyclic response of Al single crystals oriented for single slip at room temperature and demonstrated that dislocation structures are unstable upon further cyclic deformation. Ashraf and Castelluccio [20] further assimilated this transition from veins to PSBs followed by cells to an accumulation of cross slip. Similarly, experiments with small overloads [3,4,21,22] demonstrated that dislocation structures are metastable and eventually transform into cells after large enough overloads. Indeed, the saturated cyclic stress remained unchanged for low overloads, while the cyclic stress increased significantly for overloads that manage to reconfigure the structure.

This paper innovates with a framework that assumes that sufficiently large overloads destabilize the prior structures, prompting a structural reorganization. Fig. 2 schematically illustrates different possible evolutions of cyclic structures after overloads of varying magnitudes. The initial cyclic structures (veins, persistent slip bands (PSBs), cells, or Labyrinthic, which depend on prior cyclic history) will transform into new structures at different strain levels (e.g., 2%, 5%, or 10%). Mathematically, this is stated in the overload part of the flow chart in Fig. 1 (bottom right), in which the algorithm compares the structures predicted from monotonic and cyclic models and identifies the most stable dislocation structure as that with the smaller aspect ratio (η) among both loading conditions. The value of this new approach is that it relies on a comparison of internal state variables from different loading routes to identify the most likely final state without any additional information. Moreover, these internal state variables corresponds to the wall fraction and dislocation structure morphology, which are known to be material invariant and can be validated at the mesoscale with microscopy. Hence, this approach provides the means to compare the morphology of mesoscale structures and determine whether a reorganization is likely to occur after an overload. The mechanical prediction following this analysis makes predictions assuming the most stable internal state without any additional parameterization beyond those initially implemented for monotonic and cyclic modeling.

2.4. Model implementation and parameterization

The crystal plasticity model was implemented in Abaqus 2020 through a UMAT user subroutine with 8-node linear brick, reduced integration, and hourglass control elements (C3D8R) elements. A boundary condition of uniaxial tension was applied to a cubic specimen and force–displacement results extracted and converted to true strain–stress curves. Fig. 3 represents the mesh and the realistic microstructure with 101 equiaxed grains and 8788 elements used in the simulations.

A major issue for crystal plasticity models is their parameterizations, which often relies on overfitting and makes it difficult to combine monotonic and cyclic approaches. Here, we follow parameterization for monotonic and cyclic follow from the work by Dindarlou and Castelluccio [25] and Ashraf and Castelluccio [43], respectively. Tables 1 and 2 present mesoscale parameters that were previously shown to be material-independent for monotonic and cyclic loading, separately. We seek to confirm the material invariance character of the parameters under overloads by employing the same values for different metals and alloys.

Parameters that depend on the material composition relate to atomic unit processes and they are presented in Table 3. These parameters were estimated interdependently of their loading configuration, so they should be identical for monotonic and cyclic loading. Hence, the model employs the same elastic constants, glide activation energy, and thermal stress for monotonic and cyclic (which should indeed be identical), and they only differ on the dislocation structures (which should be different). Without this characteristic (which is rarely seen in models and requires individual estimation of parameters), it is not possible to combine independent monotonic and cyclic models into an overload framework.

3. Modeling results

Next, we assess the cyclic response after an overload for different crystal orientations and deformation conditions. We note that overloads not only induce changes to the bulk response, but they can also induce damage and cracking. Hence, we proceed by assuming that no cracking occurs during overloads and all damage accumulation proceeds from the cyclic deformation. Certainly, if necessary the approach presented can also be employed to evaluate fracture indicators that estimate damage during the monotonic overload.

Table 1
Cyclic mesoscale material-invariant model parameters.

Parameter	Values
Similitude coefficient, K_{struct}	2.75
Plateau plastic shear range, ΔG_M^{pl}	$1\times10^{-5}-7\times10^{-4}$
PSBs upperbound shear, ΔG_{PSB}^{pl}	0.018
The wall fraction change rate parameter, g_P	0.002
The initial wall fraction, f_0	0.45
The final wall fraction, f_{inf}	0.15
Veins aspect ratio, η_{Veins}	50.0
PSBs aspect ratio, η_{PSBs}	15.0
Cells aspect ratio, η_{Cells}	1.0
Labyrinthic aspect ratio, $\eta_{Lab.}$	5.0

Table 2
Monotonic mesoscale material-invariant parameters [25].

Parameter	Values
K_{struct}	4.05
f_w^I	0.24
f_w^{III}	0.19
η^I	4.5
ϕ	0.5
γ_{Cr}	3^{-3}

Table 3
Material-dependent parameters [25].

Parameter	Cu	NiCr
s_0^I, MPa	8	20
F_0, $\frac{KJ}{Mole}$	155	145
C_{11}, GPa	166.1	249.0
C_{12}, GPa	119.0	155.0
C_{44}, GPa	75.6	114.6

3.1. Application to cu single crystal

We first explore the response of single crystals undergoing cyclic deformation followed by monotonic overload. Such experimental data are scarce in the literature, and the work by Li et al. [21] corresponds to one of the few reported efforts. Fig. 4 presents the modeling results at the meso- and macro-scale for a Cu single crystal oriented along [017] direction, subjected to different pre-cyclic deformation. Black, red, and blue curves present the overload response after low ($\Delta\gamma_{pl} = 7\times10^{-4}$), large ($\Delta\gamma_{pl} = 3\times10^{-3}$) or prior to cyclic deformation, respectively.

Under monotonic loading without cyclic deformation, the model predicts an extended Forsyth Stage I monotonic deformation (Fig. 4a). As stated by the authors [21], the absence of an extended Stage I in their experiments is unexpected (compared to the literature) and is likely due to crystal misorientation during testing; only a few degrees can significantly change the response as shown by Dindarlou and Castelluccio [25]. Mesoscale structures on experiments correspond to walls wider spaces ($d_{struct} = 10$ μm) in Fig. 4b and elongated cells ($\eta = 8-10$) in Fig. 4c, both of which are correctly estimated by the model (Model: dotted lines, TEM estimates: dots).

The overload response predicted after low cyclic deformation ($\Delta\gamma_{pl} = 7\times10^{-4}$) exhibits both Stage I and Stage II hardening (Fig. 4a), consistent with experimental observations. Stage I hardening arises from elongated labyrinthic structures ($\eta = 5$ in Fig. 4c) formed during cyclic deformation. This structure remains stable under 5% strain overload but transforms into equiaxed cells at higher overloads ($\eta = 1$ and $d_{struct} = 1$ μm in Figs. 4b and 4c), which leads to Stage II hardening. High enough cyclic deformation ($\Delta\gamma_{pl} = 3\times10^{-3}$) form equiaxed cells that are more stable under overload conditions. As a result, smaller, more symmetric cyclic structures [4] increase initial hardening and reduce the impact of overloads.

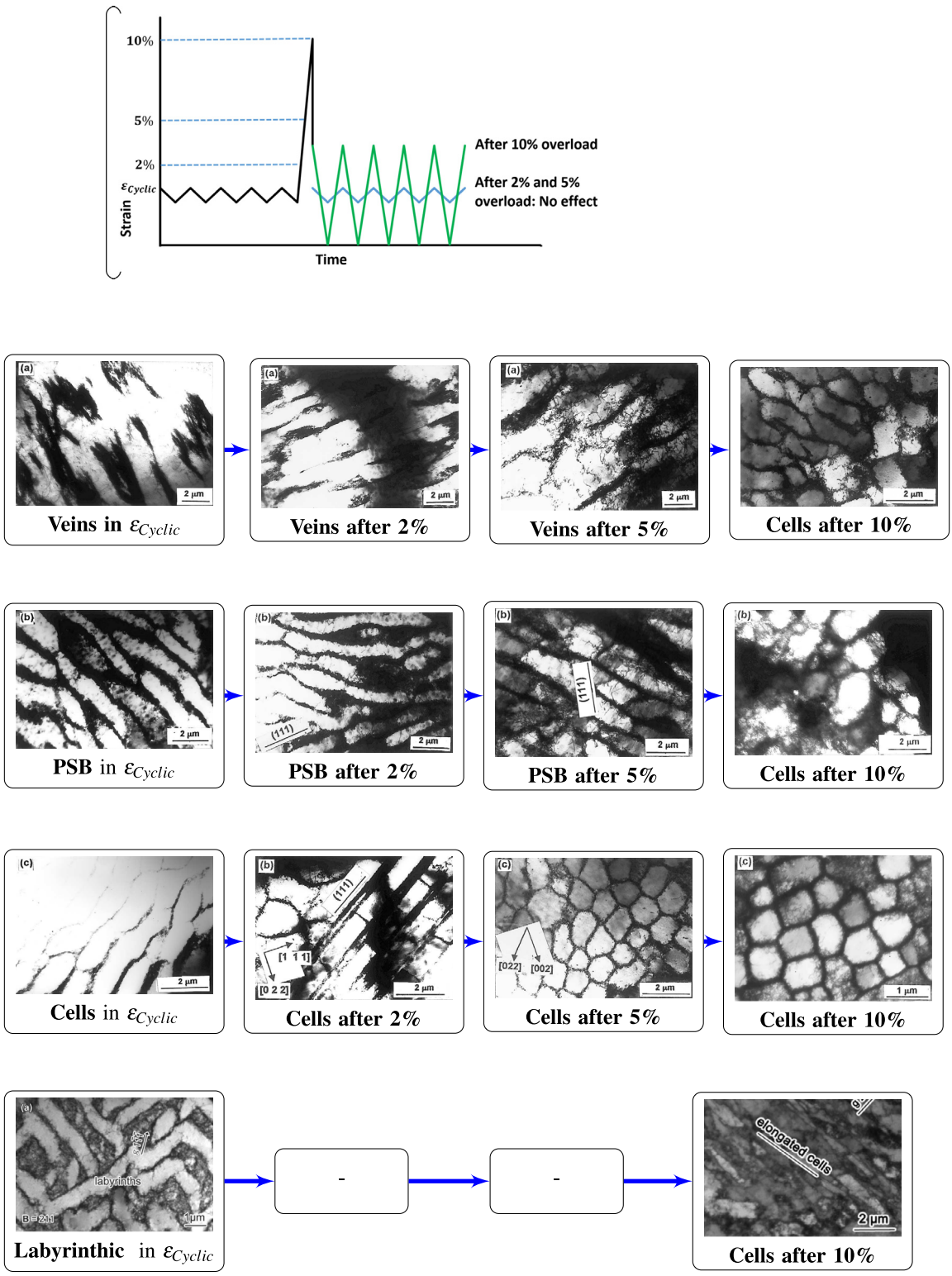

Fig. 2. Stability of various cyclic substructures during overloads. Veins, PSBs and labyrinthic substructures are stable up to five percent and transformed to stable monotonic structures (equiaxed and elongated cells) at ten percent overload. The TEM images from Ref. [4].

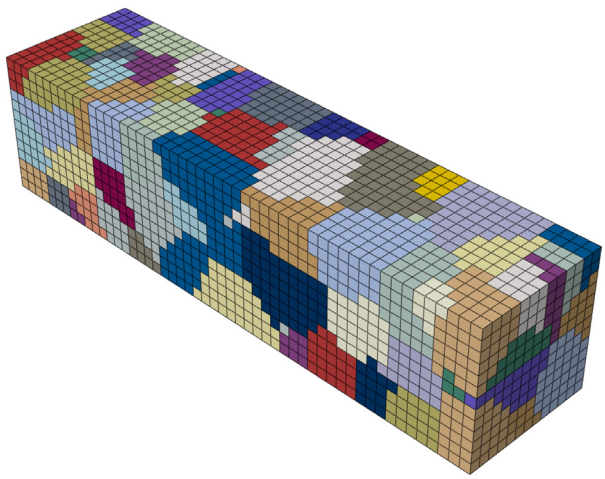

Fig. 3. Realistic microstructure and mesh with 101 equiaxed grains, 8788 elements and uniaxial loading. On one end nodes are restricted to move in the axial direction while on the other end their are displaced under strain control.

3.2. Application to cu polycrystal

Fig. 5a and 5b compare experimental and modeling saturated cyclic stress strain curves (CSSC) for Cu polycrystals after five and ten percent overstrains, respectively. At five percent strain, the CSSC increases only at low cyclic strains, for which the monotonic excursion results in a finer structure than the stable cyclic structure. At higher cyclic strains, the structure is already finer that the from the overstain, so there is almost no change. At 10 percent overstain, the CSSC increases for all strain amplitudes. We highlight that no reparameterization was required, since the prediction arises from comparing the stability of independent dislocation structures from monotonic or cyclic loading, which were calibrated independently from the overload experiment.

Fig. 6a, 6c and 6e present the dislocation structures predicted by the model for fatigue, five and ten percent overstrain samples, respectively. The larger monotonic excursion results in a larger portion of grains occupied by cells. The predicted structure transformations are consistent with TEM images in Fig. 6b, 6d and 6f. Therefore, at low cyclic strains, veins and PSBs dominate while cells and labyrithic structure do at high cyclic strains. After a low overload, the transition to cell structures dominate the response at low cyclic strains and no significant changes appear at higher cyclic strains, for which the intrinsic structure is already more stable. For large overloads, cells refine the stable cyclic structure for all strain ranges.

3.3. Application to nicr alloy polycrystal

The approach is now applied to predict the overload response of polycrystalline NiCr alloy (single phase FCC with solid solution strengthening) by making use of material invariant parameters in Tables 1 and 2, and the elastic properties and dislocation glide parameters in Table 3. Fig. 7 represents blind predictions of monotonic, cyclic, and overload response of NiCr polycrystal. Predicted and experimental mesoscale structures presented in Fig. 8a, 8b and 8c demonstrate that elongated structures refined after a 14% overload. It is worth noticing that this model employs the same parameters F_0 and S_0 for Cu and does not require any additional calibration using the experimental overload data.

4. Discussion

Rather than proposing a new model fit to limited overload data, this paper assesses the predictive power of substructure-sensitive models and their parameterizations using a novel strategy that compares dislocation structures morphologies. Hence, this work demonstrates that models capture the response under complex loading conditions beyond the initial validation, and importantly, without changing the parameterization from monotonic and cyclic loading independently. The resulting model can predict dislocation substructures effectively without additional fitting or characterization. Thus, the approach allows to explore confidently overload scenarios without requiring a specific overload test required for calibration. By further relying on material-invariant parameters calibrated from proxy materials, this work provides a route to reduce experimental needs and accelerate damage prognosis.

Our analysis has also demonstrated that the mechanical response after combining monotonic and cyclic deformation in single phase FCC materials strongly depends on the dominant dislocation structures. By comparing the dimensions of the substructures generated through independent loading routes, the novel approach in Fig. 1 predicts the response after overloads without any reparameterization. Notably, we the approach effectively relies on material-invariant mesoscale parameters, which reduce the need for additional testing to rank overloads effects for new materials and loading conditions.

Next, we employ the model to explore fatigue crack initiation in single- and poly-crystals after an overload for which almost no experimental data is available. Here, we refer to initiation as the number of cycles to crack first grain. We note that even when we focus on a single overload, the approach is general enough to be applicable to a sequence of random overloads to quantify damage accumulation without any additional provision. Moreover, the approach can validate or improve cyclic counting methods, such as Rainflow algorithm [45], by determining their accuracy for different microstructures or crystallographic textures.

4.1. Effect of overloads on crystal orientation

No experimental study has comprehensively explored the roles of overloads in cyclic deformation at different strain levels and for single crystals of different orientations. Fig. 9 presents the model estimates for the cyclic deformation of Cu single crystals with different orientations and overloads levels. While a five percent overload is not sufficient to refine the PSB structure in crystals loaded along a [112] direction, a ten percent overload is enough to transform the structures to elongated cells and increase the cyclic stress (Fig. 9a). In [110] crystals with longer hardening Stage I, higher overloads are needed to change the structure into cells and increase the cyclic stress (Fig. 9b). Labyrinthic structure in [100] crystal are less stable in Fig. 9c and converts to cells after five percent overload. Since the change of dislocation structure aspect ratio in [112] and [110] crystals is larger than the change in [100] crystal ($\eta^{PSB} \rightarrow \eta^{I} > \eta^{Lab} \rightarrow \eta^{III}$), the increase of the stress due to overload is higher. However, cell structures in [111] crystals are stable even after large overloads, and the cyclic stress remains unchanged in Fig. 9d. These results support that the effects of overloads would be low for textured polycrystals with more grains near multiple slip orientations and their fatigue lives would not be significantly altered. Moreover, polycrystals with rolling texture dominated by [111] and [100] orientations are less susceptible to overloads affecting the cyclic response than those dominated by single-slip oriented grains, specially at low strain amplitudes. This analysis is consistent with trends found on experiments [46,47].

4.2. Effect of overloads on fatigue crack initiation

Since grains oriented for single slip are preferred sites for fatigue crack initiation [52], our analysis suggests that overloads will have a significant effect on early fatigue lives, specially in the high cycle fatigue regime. This rationale aligns with experimental evidence [53, 54], which demonstrated that overloads have a dominant effects at low strain amplitudes in the so-called threshold regime. In this case, long

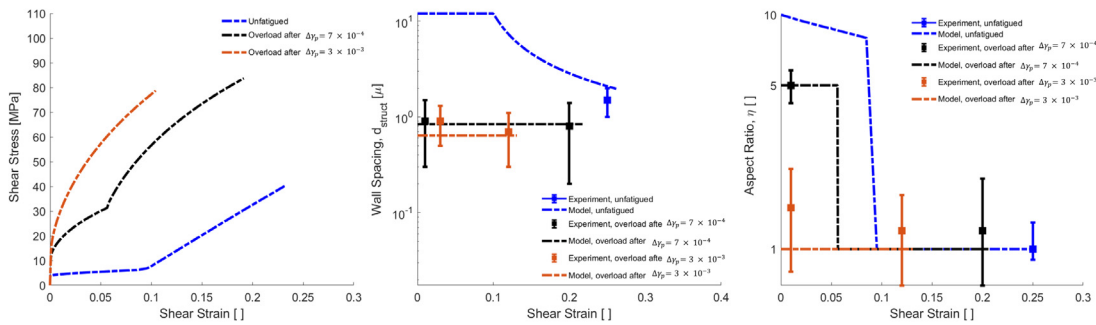

(a) (b) (c)

Fig. 4. Meso- and macro-scale overload response of [017] Cu single slip crystal, subjected to different pre-cyclic deformation. Blue, black, and red curves demonstrate the overload response without (unfatigued), after low, and after high cyclic deformation, respectively (low 7×10^{-4} and high 3×10^{-3} cyclic plastic strain, $\Delta\gamma_{pl}$). (a) Predicted stress–strain curves, (b) Walls spacing, d_{struct}, (c) Substructure aspect ratio, η. Experiments from Ref. [21].

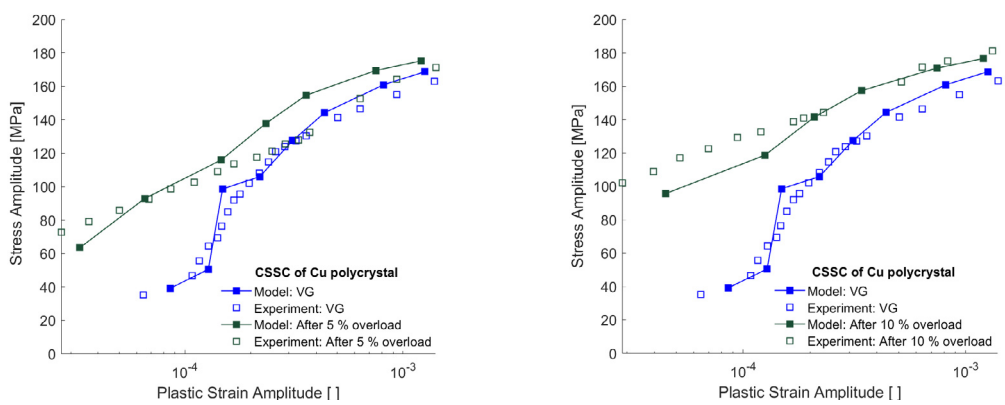

(a) (b)

Fig. 5. Increase of saturated cyclic stress of Cu polycrystal and transformation of mesoscale structures by five and ten percent overloads. CSSCs of virgin (VG) Cu polycrystals after (a) Five and (b) Ten percent overload. The macroscopic stress increase by the overloads coincides with mesoscale structure transformations. The experimental data from Ref. [3].

cracks encompass multiple grains oriented for single- and multiple-slip, which moderate overload effects.

To quantify the effects of overloads on crack initiation, we consider FIPs, which are microstructural surrogates of the fatigue crack initiation driving force [55,56]. Specifically, we evaluate the effect of overloads on fatigue initiation by considering the FIP proposed by Fatemi and Socie [57] and later reformulated at the slip-system level by Castelluccio and McDowell [58], i.e.,

$$FIP_{FS} = \Delta\gamma^{\alpha}_{max}\left[1 + k\frac{\sigma_n^{max}}{\sigma_y}\right], \tag{25}$$

where $\Delta\gamma^{\alpha}_{max}$ is the maximum cyclic plastic shear strain among all slip systems, k is a normalization constant, σ_n^{max} is the maximum normal stress on the maximum plastic shear range plane, and σ_y is the reference strength (we used $\sigma_y = 150$ MPa for Cu and $k = 0.5$ in this work).

Next, we use the polycrystal model in Fig. 3 and Eq. (25) to compute the FIPs for every slip system and element during the first cycle after an overload. These values are then averaged for each grain, such that each results in 12 different grain-averaged FIPs, one per slip system. Fig. 10 presents the grain-averaged FIPs for Cu taking into account the pristine material, as well as five and ten percent overloads; we also consider size levels of cyclic shear strains. The results demonstrate that at low cyclic plastic strains, overloads can significantly reduce the FIPs thanks to a transformation of elongated cyclic structures (veins and PSBs) into refined monotonic cells. We note that overloads affect both the mean and the extremes of the FIP distributions, the latter of which controls fatigue crack initiation.

We further evaluate the correlation between the FIP following an overload and the initial apparent Schmid factor. The results in Fig. 11 show that FIPs increase with the Schmid factor for cyclic deformation, but not for overloads, particularly at low cyclic strain levels. Certainly, overloads reduce or even eliminate the positive correlation between FIPs and apparent Schmid factor. Hence, these results suggest that fatigue crack initiation under low amplitude fatigue following an overload may be driven by grains oriented for both, low and high apparent Schmid factors. This result adds to the sources of uncertainty affecting fatigue lives during service and helps to explain the experimental fact that cracks not always initiate in high Schmid factor grains.

Finally, Fig. 12 represents the effect of the overloads on the fatigue life following the correlation between FIP and fatigue life ($N_{nuc} \propto FIP^{-2}$) proposed by Castelluccio and McDowell [58]. Here, we consider the maximum FIP among all grains to estimate the most critical fatigue crack initiation event. Our analysis suggests that large enough overloads can increase the number of cycles to initiate a fatigue crack by up to two orders of magnitudes. The largest life gains occur for low strains amplitudes in which long structures (Veins, PSBs and Lab.) transform into cells, which are not naturally formed during low amplitude cyclic deformation. The increase in fatigue lives from overloads agree with the experimental trends reported, in which the threshold regime is more sensitive to overloads [3,4,7–10,12–14,21,22].

5. Conclusion

This work presents a novel framework to estimate the cyclic response following overloads in the absence of dedicated experimental

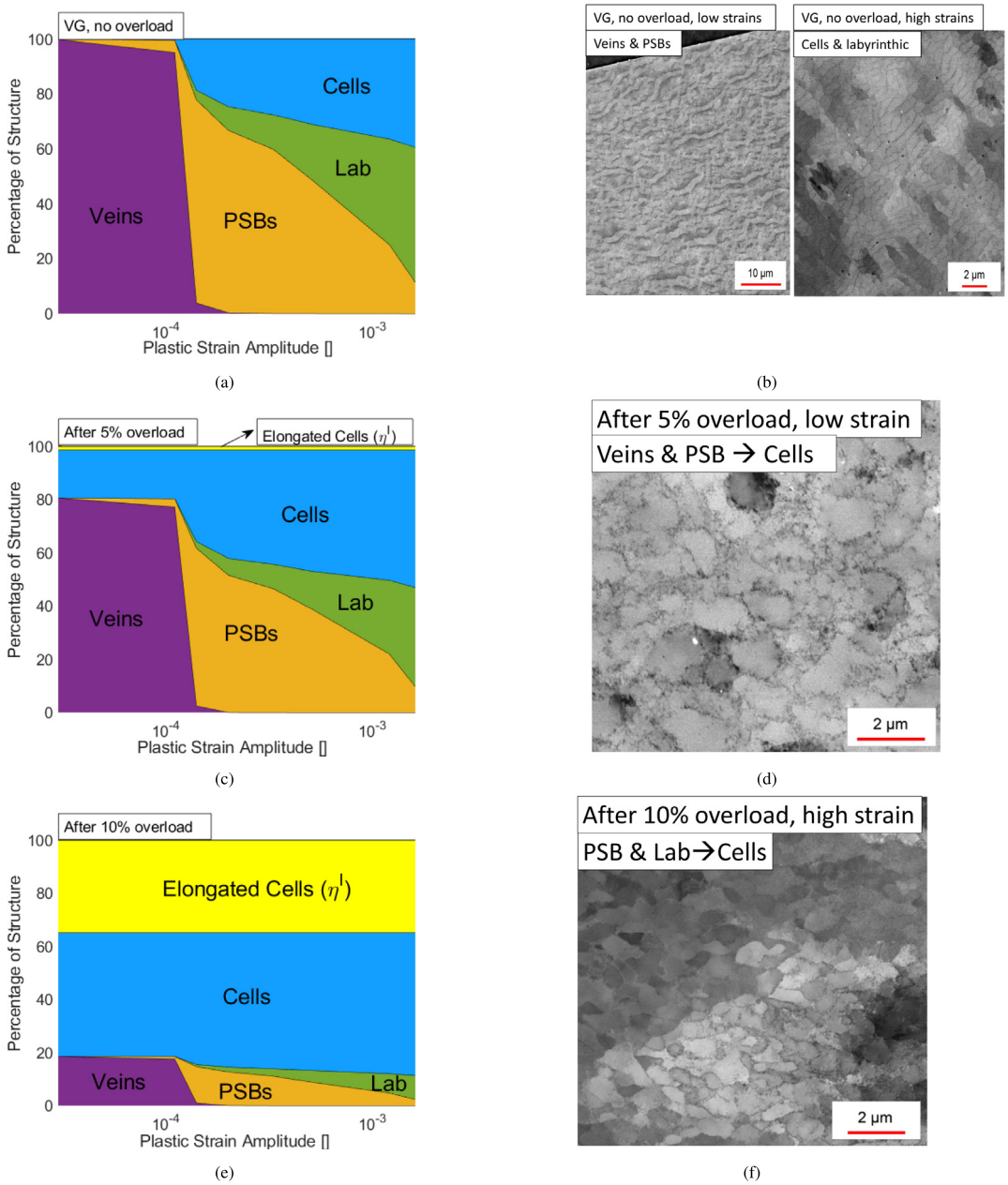

Fig. 6. Mesoscale structures predicted for (a–b) VG sample, and after (c–d) Five and (e–f) Ten percent overloads agree with TEM images in d, g and h. Transformation of pre-cyclic long structures (Veins, PSBs and Labyrinthic) to refined cells and Type I structure, by the overloads, raises the macroscopic stress. The experimental data from Ref. [3].

data. The approach is based on evaluating the stability of dislocation structures under further deformation and their potential for refinement. The framework combines substructure-based crystal plasticity (CP) models for FCC single-phase materials parameterized for monotonic and constant periodic loading in order to predicted the influence of overloads on subsequent cyclic deformation. The models utilizes the same mesoscale parameters across different materials, demonstrating that complex loading sequences can be effectively modeled using the principle of parameter material invariance for single- and poly-crystals. Overall, predictions for macroscopic stress–strain behavior and mesoscale structure morphology are consistent with experimental results for both single- and poly-crystals.

The analysis further demonstrated that the cyclic response after an overload is influenced by cyclic history and crystal orientation. In single crystals oriented for single slip, prior cyclic deformation can lead to a reduction or complete disappearance of monotonic Stage I, depending on the initially applied cyclic strain range. The higher hardening rates and the earlier onset of Stage II under monotonic loading were attributed to the development of more refined and stable mesoscale structures during previous cyclic loading.

The effects of an overload on subsequent cyclic behavior depend on the level of deformation and crystal orientation. Sufficiently large overloads (ranging from 5% to 30%, depending on the orientation) can induce a transformation from elongated to equiaxed structures, altering the cyclic response. In polycrystalline metals and alloys, a similar transformation from elongated structures to equiaxed cells following an overload leads to an increase in the saturated cyclic stress, in agreement with experimental results. The comparison of the dominant substructures predicted by the model and those observed in experiments provided a mesoscale validation of the approach.

Finally, the model evaluates the likelihood of fatigue crack initiation by analyzing changes in grain-averaged FIPs after overloads. The results show that the impact of overloads on fatigue life is highly dependent on crystal orientation and the magnitude of the overload.

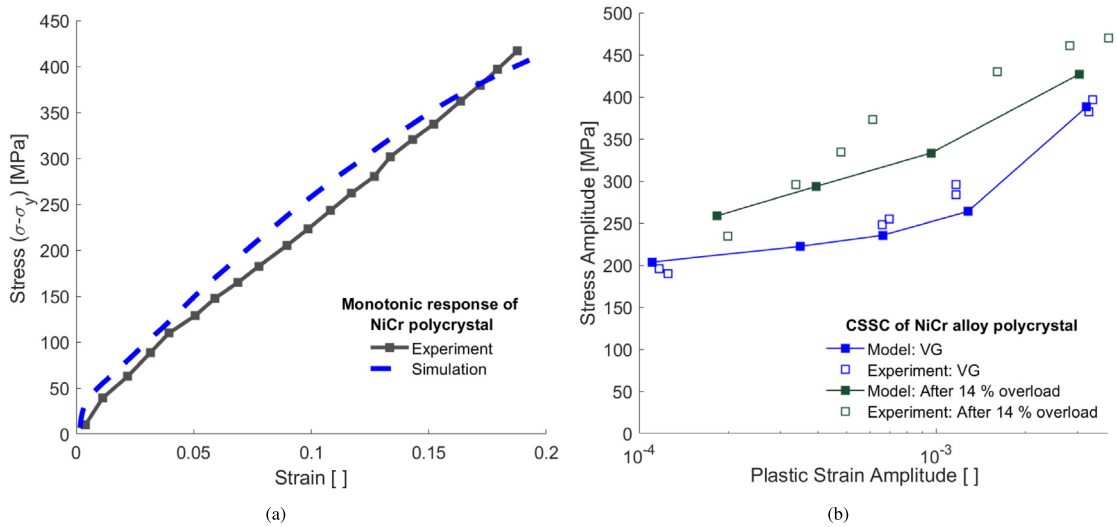

Fig. 7. (a) Prediction of monotonic response of NiCr polycrystal. (b) CSSCs of virgin (VG) material and after 14 percent overload of this alloys. Experiments from Refs. [2,44].

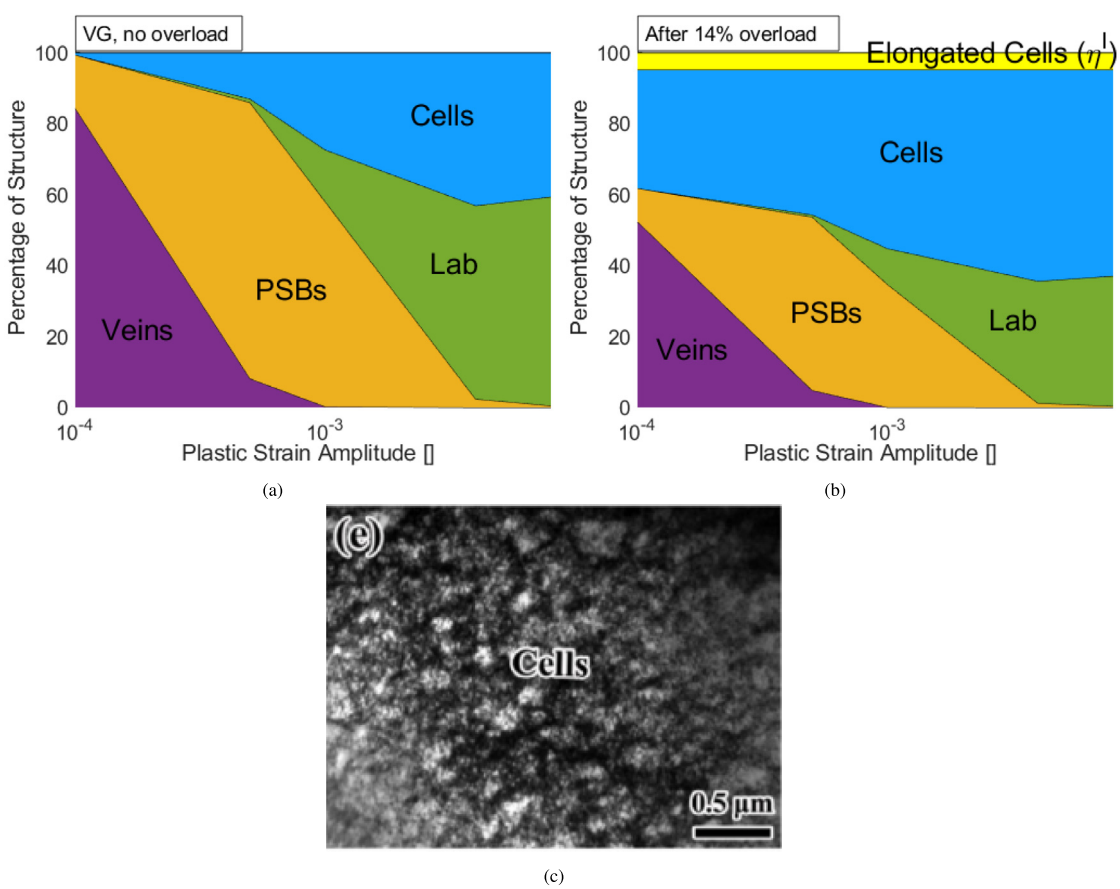

Fig. 8. Predicted mesoscale structures for VG sample (a), and after 14 percent overload (b) and (c) TEM image showing the refined structure after the overload. The transformation of long structures to cells by the overload increases the stress. Experiments from Refs. [2,44].

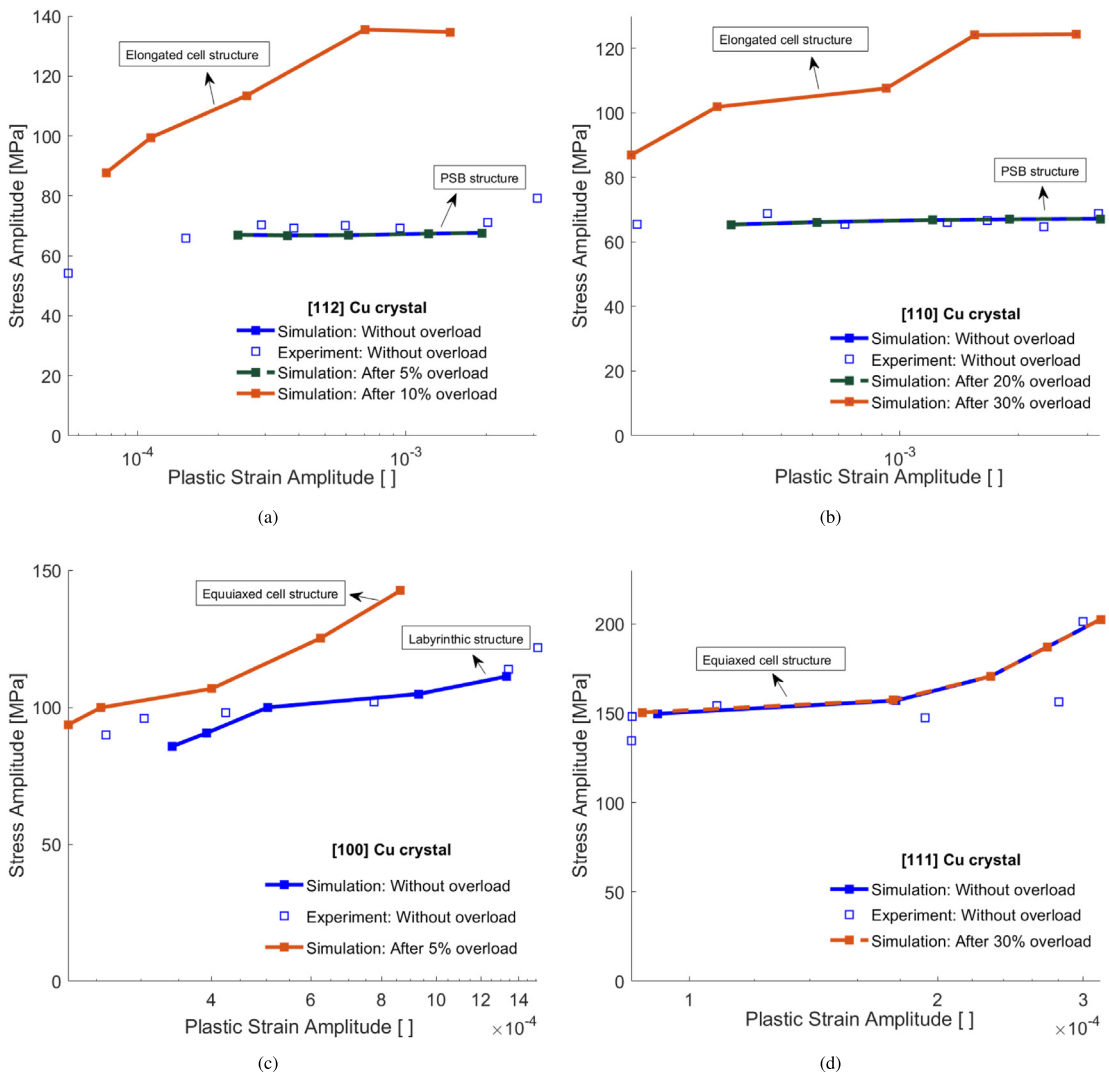

Fig. 9. Predicted effects of overloads on cyclic deformation for (a) [112] (b) [110] (c) [100] and [111] Cu single crystals. While five percent overload is not sufficient to change the structure in [112] crystal, PSBs formed in pre-cycles transformed to elongated cells in ten percent overload. In [110] crystal with longer hardening Stage I, higher overloads are needed to change the structure. Accordingly, PSBs are stable even after 20 percent but altered to elongated cells after 30 percent overload. Labyrinthic structure in [100] crystal is changed to equiaxed cells even in five percent overload. Cell structure in [111] multiple slip crystal is stable even after 30 percent overload and stress remained unchanged. Experiments from Refs. [48–51].

An overload under small amplitude fatigue is more likely to modify the dislocation substructure and hence improve the fatigue life than under large amplitude deformation. Furthermore, the analysis suggests that overloads can enhance the fatigue life of polycrystalline materials with grains predominantly oriented for single-slip, especially in the high-cycle fatigue regime. As a result, fatigue crack initiation within a grain can be delayed by several orders of magnitude in this regime and overloads make crack initiation in low apparent Schmid factor grains more likely.

CRediT authorship contribution statement

Shahram Dindarlou: Writing – original draft, Software, Methodology, Data curation. **Gustavo M. Castelluccio:** Writing – review & editing, Writing – original draft, Supervision, Investigation, Funding acquisition, Formal analysis, Conceptualization.

Funding

GMC thanks The EPSRC, UK for funding under EPSRC grant EP/R034478/1.

Code availability

The codes that support the findings of this study are available from the corresponding author upon reasonable request.

Declaration of competing interest

The authors declare that they have no known competing financial interests or personal relationships that could have appeared to influence the work reported in this paper.

Data availability

Data will be made available on request.

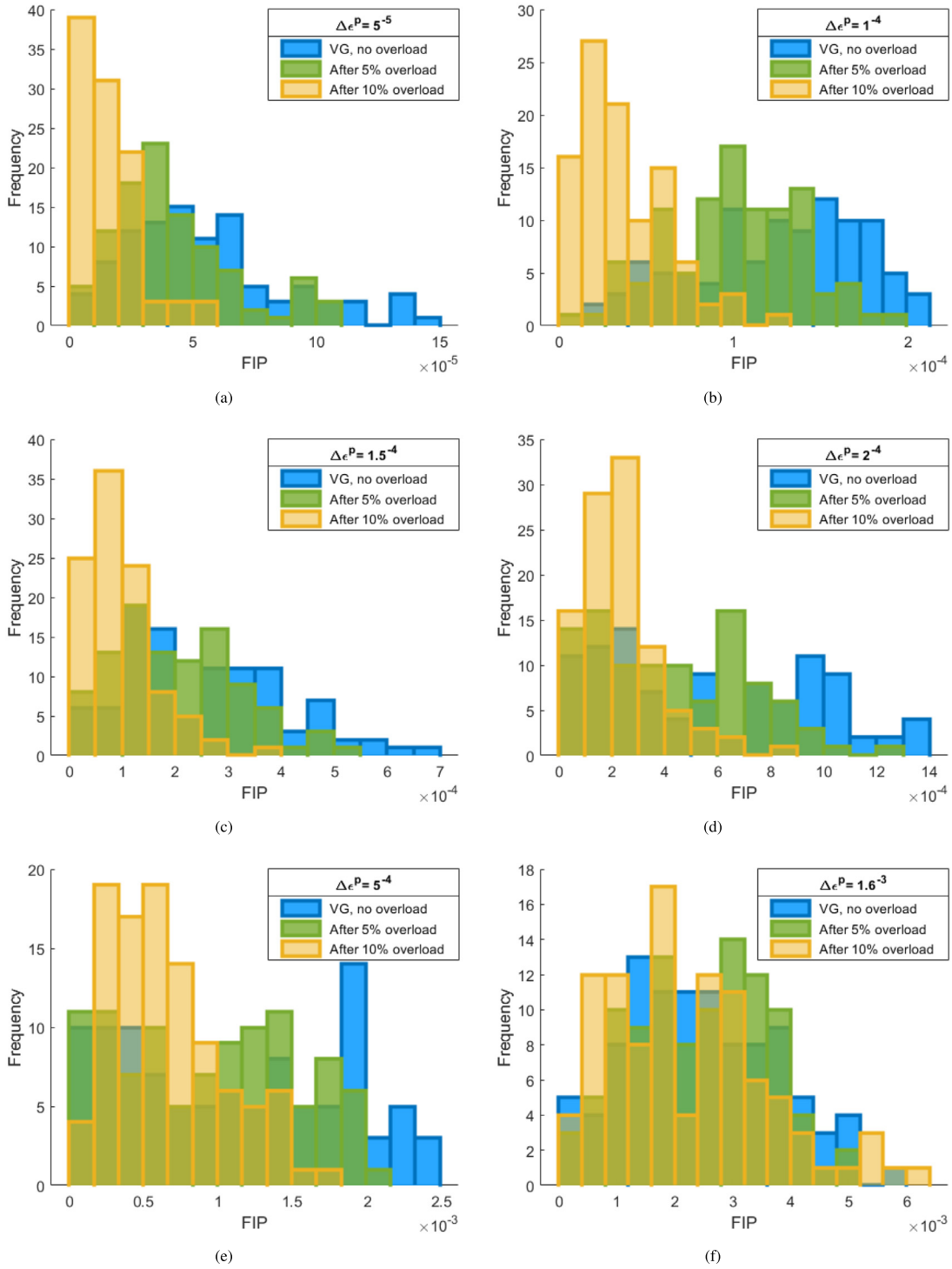

Fig. 10. Predicted effects of the overloads on the averaged-per-grain FIPs at different cyclic plastic strains for Cu polycrystal. FIP distributions decrease by the overload. This reduction is more prevalent at low cyclic plastic strains where more long structures (veins and PSBs) transform to refined cells by the overload.

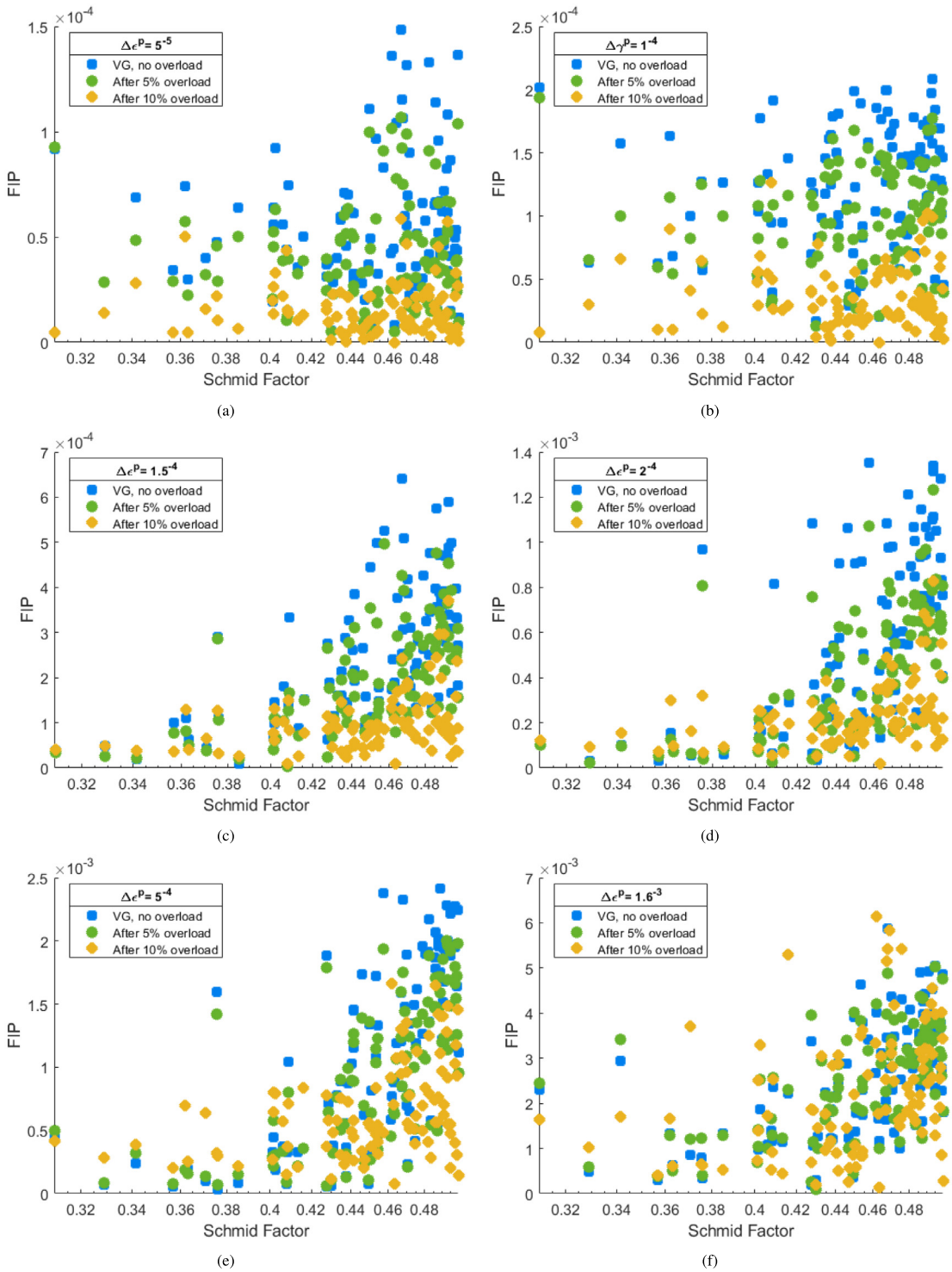

Fig. 11. Predicted effects of the overloads on the averaged-per-grain FIPs for differently oriented grains (apparent Schmid factors) at various cyclic plastic strains for Cu polycrystal. The overloads affect mostly the single slip grains with high Schmid factors.

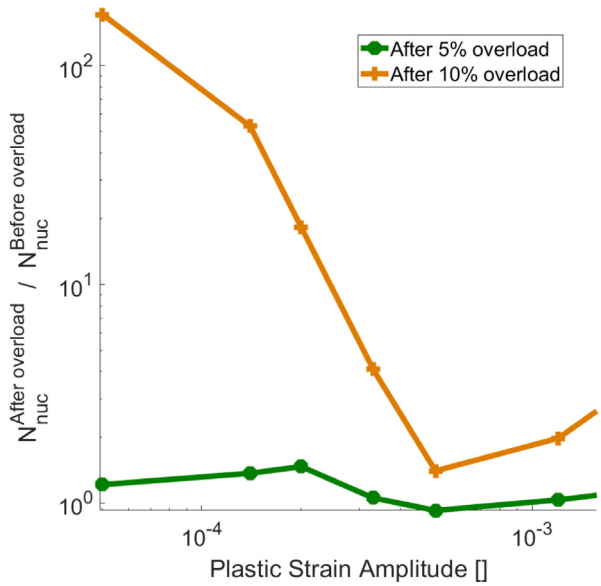

Fig. 12. The effect of the overloads on the fatigue life as a function of the plastic strain amplitude. We used the maximum value of FIP among all elements to consider the most critical fatigue life assessment ($N_{nuc} \propto FIP_{max}^{-2}$). Large enough overloads, modify fatigue life by transforming long structures (Veins, PSBs and Lab.) to cells, which are finer structures.

References

[1] Dieter G, Bacon D. Mechanical metallurgy. vol. 3, New York: Mc Graw-Hill Book Co.; 1976.

[2] Marnier G, Keller C, Taleb L. Tensile prestrain memory effect on subsequent cyclic behavior of fcc metallic materials presenting different dislocations slip modes. Int J Plast 2016;78:64–83. http://dx.doi.org/10.1016/j.ijplas.2015.11.001.

[3] Marnier G, Keller C, Taleb L. Fatigue of OFHC pure copper and 316l stainless steel subjected to prior tensile and cyclic prestrains. Int J Fatigue 2016;91:204–19. http://dx.doi.org/10.1016/j.ijfatigue.2016.06.009.

[4] Jia W, Fernandes J. Mechanical behaviour and the evolution of the dislocation structure of copper polycrystal deformed under fatigue-tension and tension-fatigue sequential strain paths. Mater Sci Eng A 2003;348(1–2):133–44. http://dx.doi.org/10.1016/S0921-5093(02)00630-5.

[5] Kunz L, Lukáš P, Weiss B, Melisova D. Effect of loading history on cyclic stress–strain response. Mater Sci Eng A 2001;314(1–2):1–6. http://dx.doi.org/10.1016/S0921-5093(00)01922-5.

[6] Mahato J, De P, Sarkar A, Kundu A, Chakraborti P. Effect of prestrain and stress rate on bauschinger effect of monotonically and cyclically deformed ofhc copper. Procedia Eng 2014;74:368–75. http://dx.doi.org/10.1016/j.proeng.2014.06.281.

[7] Voorwald HJ, Torres MA, Pinto Júnior CC. Modelling of fatigue crack growth following overloads. Int J Fatigue 1991;13(5):423–7. http://dx.doi.org/10.1016/0142-1123(91)90600-4.

[8] Seifi R, Bahrami R. Numerical modeling the effects of overloading and underloading in fatigue crack growth. Eng Fail Anal 2010;17(6):1475–82. http://dx.doi.org/10.1016/j.engfailanal.2010.05.009.

[9] Higo Y, Nunomura S. The effect of a single peak overload on fatigue crack propagation rate and crystallographic path in Fe-3% si single crystals. Acta Metall 1984;32(7):1029–34.

[10] Bahloul A, Bouraoui C. The overload effect on the crack-tip cyclic plastic deformation response in SA333 gr 6 C-mn steel. Theor Appl Fract Mech 2019;99:27–35.

[11] Castelluccio GM, Musinski WD, McDowell DL. Recent developments in assessing microstructure-sensitive early stage fatigue of polycrystals. In: Slip localization and transfer in deformation and fatigue of polycrystals, Curr Opin Solid State Mater Sci In: Slip localization and transfer in deformation and fatigue of polycrystals, 2014;18(4):180–7. http://dx.doi.org/10.1016/j.cossms.2014.03.001.URL http://www.sciencedirect.com/science/article/pii/S1359028614000163,

[12] Goel H, Chand S. A fatigue crack growth model for single overload tests. J Eng Mater Technol 1994;116(2):168–72. http://dx.doi.org/10.1115/1.2904268.

[13] Mehrzadi M, Taheri F. A material sensitive modified wheeler model for predicting the retardation in fatigue response of AM60b due to an overload. Int J Fatigue 2013;55:220–9.

[14] Jones R. Fatigue single-cycle growth retardation after peak overload in ti-6AI-4v titanium. Eng Fract Mech 1973;5:585–604.

[15] Li Y, Aubin V, Rey C, Bompard P. Polycrystalline numerical simulation of variable amplitude loading effects on cyclic plasticity and microcrack initiation in austenitic steel 304L. Fatigue Damage Struct Mater VIII 2012;42:71–81. http://dx.doi.org/10.1016/j.ijfatigue.2011.07.003, URL http://www.sciencedirect.com/science/article/pii/S0142112311001861.

[16] Li Y, Aubin V, Rey C, Bompard P. The effects of variable stress amplitude on cyclic plasticity and microcrack initiation in austenitic steel 304L. Proc the 21st Int Work Comput Mech Mater (IWCMM 21) 2012;64:7–11. http://dx.doi.org/10.1016/j.commatsci.2012.05.028, URL http://www.sciencedirect.com/science/article/pii/S0927025612002996.

[17] Xie C, Sun T, Li L, Zheng Z. Effect of Microstructure on Fatigue Damage Accumulation in 7075 Aluminum Alloy Subjected to a Single Compressive Overload. Metals 2024;14(9):980. http://dx.doi.org/10.3390/met14090980, URL https://www.mdpi.com/2075-4701/14/9/980, Number: 9 Publisher: Multidisciplinary Digital Publishing Institute.

[18] Xie C, Zheng Z, Li L, Sun T. The Overload Effect on the Crack Tip Damage Mechanism in a 7075 Aluminum Alloy. Materials 2024;17(16):4088. http://dx.doi.org/10.3390/ma17164088, URL https://www.mdpi.com/1996-1944/17/16/4088, Number: 16 Publisher: Multidisciplinary Digital Publishing Institute.

[19] Jiang YY, Zhang JX. Benchmark experiments and characteristic cyclic plasticity deformation. Int J Plast 2008;24(9):1481–515. http://dx.doi.org/10.1016/j.ijplas.2007.10.003.

[20] Ashraf F, Castelluccio G. History and temperature dependent cyclic crystal plasticity model with material-invariant parameters. Int J Plast 2023;161:103494.

[21] Li X, Wang X, Guo W, Qi C, Yan Y. Effect of cyclic predeformation on the uniaxial tensile deformation behavior of [017] cu single crystals oriented for critical double slip. Met Mater Trans A 2013;44(4):1631–5. http://dx.doi.org/10.1007/s11661-013-1625-y.

[22] Li X, Wang X, Yan Y, Guo W, Qi C. Effect of pre-fatigue on the monotonic deformation behavior of a coplanar double-slip-oriented cu single crystal. Metals 2016;6(11):293. http://dx.doi.org/10.3390/met6110293.

[23] Castelluccio G, McDowell D. Mesoscale cyclic crystal plasticity with dislocation substructures. Int J Plast 2017;98:1–26. http://dx.doi.org/10.1016/j.ijplas.2017.06.002.

[24] Dindarlou S, Castelluccio G. Substructure-sensitive crystal plasticity with material-invariant parameters. Int J OfPlasticity 2022;155.

[25] Dindarlou S, Castelluccio G. Optimization of crystal plasticity parameters with proxy materials data for alloy single crystals. Int J Plast 2024;174:103894.

[26] Rice J. Inelastic constitutive relations for solids: An internal-variable theory and its application to metal plasticity. J Mech Phys Solids 1971;28(9):877. http://dx.doi.org/10.1038/nbt0910-877.

[27] Peirce D, Asaro R, Needleman A. Material rate dependence and localized deformation in crystalline solids. Acta Metall 1983;31(12):1951–76. http://dx.doi.org/10.1016/0001-6160(83)90014-7.

[28] Orowan E. Problems of plastic gliding. Proc Phys Soc (1926- 1948) 1940;52(1):8.

[29] Krausz AS, Eyring H. Chemical Kinetics of Plastic Deformation. J Appl Phys 1971;42(6):2382–5. http://dx.doi.org/10.1063/1.1660552.

[30] Mott N, Nabarro F. Dislocation theory and transient creep in" strength of metals. 1947.

[31] Fleischer R. Rapid solution hardening, dislocation mobility, and the flow stress of crystals. J Appl Phys 1962;33(12):3504–8. http://dx.doi.org/10.1063/1.1702437.

[32] Dunne F, Rugg D, Walker A. Lengthscale-dependent, elastically anisotropic, physically-based hcp crystal plasticity: Application to cold-dwell fatigue in Ti alloys. 2007;23:1061–83. http://dx.doi.org/10.1016/j.ijplas.2006.10.013.

[33] Langer J. Statistical thermodynamics of crystal plasticity. J Stat Phys 2019;175(3–4):531–41. http://dx.doi.org/10.1007/s10955-019-02221-7.

[34] Kocks U, UF K, A.S. A, M.F. A. Thermodynamics and kinetics of slip. Prog Mater Sci 1975;19:1–47.

[35] Devincre B, Hoc T, Kubin L. Dislocation mean free paths and strain hardening of crystals. Science 2008;1688:61–4.

[36] Mura T. Micromechanics of defects in solids. Springer Science & Business Media; 2013.

[37] Ashraf F, Castelluccio G. On the similitude relation for dislocation wall thickness under cyclic deformation. Mater Sci Eng A 2022;142972.

[38] Sauzay M, Kubin L. Scaling laws for dislocation microstructures in monotonic and cyclic deformation of fcc metals. Prog Mater Sci 2011;56(6):725–84. http://dx.doi.org/10.1016/j.pmatsci.2011.01.006.

[39] Kubin L, Sauzay M. Persistent slip bands: Similitude and its consequences. Acta Mater 2016;104:295–302.

[40] Lin P, Vivekanandan V, Castelluccio G, Anglin B, El-Azab A. Crystal plasticity-inspired statistical analysis of dislocation substructures generated by continuum dislocation dynamics. Comput Mater Sci 2021.

[41] Mughrabi H, Ackermann F, Herz K. Persistent slipbands in fatigued face-centered and body-centered cubic metals. In: Fatigue mechanisms. STP 675, ASTM; 1979, p. 69–105.

[42] Dhers J, Driver J. The cyclic response and microstructures of aluminium single crystals. Mater Sci Monogr 1988;46:33–40.

[43] Ashraf F, Castelluccio G. A robust approach to parameterize dislocation glide energy barriers in FCC metals and alloys. J Mater Sci 2021;56(29):16491–509.
[44] Zhang Y, Han D, Li XW. A unique two-stage strength-ductility match in low solid-solution hardening Ni-Cr alloys: decisive role of short range ordering. Scr Mater 2020;178:269–73.
[45] Suresh S. Fatigue of materials, second ed.. Cambridge solid state science series, Cambridge University Press; 1998.
[46] Li Y. Fatigue crack initiation (in 304L steel) : influence of the microstructure and variable amplitude loading - TEL - thèses en ligne (Ph.D. thesis), Ecole Centrale Paris; 2012, URL https://theses.hal.science/tel-00697002/.
[47] Saalfeld S, Scholtes B, Niendorf T. On the influence of overloads on the fatigue performance of deep rolled steel SAE 1045. Int J Fatigue 2019;126:221–30. http://dx.doi.org/10.1016/j.ijfatigue.2019.05.001.
[48] Li X, Zhang Z, Wang Z, Li S, Umakoshi Y. SEM-ECC investigation of dislocation arrangements in cyclically deformed copper single crystals with different crystallographic orientations. In: Defect and diffusion forum. 188, Trans Tech Publ; 2001, p. 153–70.
[49] Li X, Wang Z, Li G, Wu S, Li S. Cyclic stress–strain response and surface deformation features of [011] multiple-slip-oriented copper single crystals. Acta Mater 1998;46(13):4497–505.
[50] Gong B, Wang Z, Wang Z. Cyclic deformation behavior and dislocation structures of [001] copper single crystals—I cyclic stress-strain response and surface feature. Acta Mater 1997;45(4):1365–77.
[51] Li X, G. Wang Z, Li S. Influence of crystallographic orientation on cyclic strain-hardening behaviour of copper single crystals. Phil Mag Lett 1999;79(11):869–75.
[52] Kakandar E, Barrios A, Michler J, Maeder X, Pierron ON, Castelluccio GM. A computational and experimental comparison on the nucleation of fatigue cracks in statistical volume elements. Int J Fatigue 2020;137:105633. http://dx.doi.org/10.1016/j.ijfatigue.2020.105633, URL http://www.sciencedirect.com/science/article/pii/S014211232030164X.
[53] Seifi R, Mohammadi MR. Effects of tensile overload on crack initiation life and fatigue crack growth in notched specimens. Trans Indian Inst Met 2018;71(9):2339–48. http://dx.doi.org/10.1007/s12666-018-1365-1.
[54] Seifi R, Mohammadi MR. Effects of initial overload on the fatigue crack initiation and growth in notched plates. Theor Appl Fract Mech 2024;131:104433. http://dx.doi.org/10.1016/j.tafmec.2024.104433, URL https://www.sciencedirect.com/science/article/pii/S0167844224001824.
[55] Castelluccio G. A study on the influence of microstructure on small fatigue cracks. Georgia Institute of Technology; 2012.
[56] Castelluccio G, McDowell D. Assessment of small fatigue crack growth driving forces in single crystals with and without slip bands. Int J Fract 2012;176(1):49–64.
[57] Fatemi A, Socie D. A critical plane approach to multiaxial fatigue damage including out-of-phase loading. Fatigue Fract Eng Mater Struct 1988;11(3):149–65.
[58] Castelluccio G, McDowell D. A mesoscale approach for growth of 3D microstructurally small fatigue cracks in polycrystals. Int J Damage Mech 2014;23(6):791–818.